Hindawi
International Journal of Aerospace Engineering
Volume 2020, Article ID 1327848, 17 pages
https://doi.org/10.1155/2020/1327848

Research Article

Study on Mechanical Properties of Submunition's Ribbon Straightening Section

Dong-ze Qin,[1] **Wei Zhang**,[1,2] **Shu-Yun Zhang**,[3] **Tian-Ji Guo**,[4] **Shui-Yuan Pei**,[1] **and Jin-Shi Zhang**[1]

[1]*School of Mechatronic Engineering, North University of China, Taiyuan 030051, China*
[2]*Advanced Manufacturing Technology Laboratory in Shanxi, North University of China, Taiyuan 030051, China*
[3]*Shanxi North Machine-Building Co., Ltd, Taiyuan 030009, China*
[4]*Beijing Institute of Space Long March Vehicle, Beijing 100076, China*

Correspondence should be addressed to Dong-ze Qin; apo1981@126.com

Received 11 June 2019; Accepted 18 December 2019; Published 20 January 2020

Academic Editor: Rosario Pecora

The humanitarian damage caused by the unexploded submunitions is one of the hot issues of concern to the international community at present. A portion of the submunition that did not explode was caused by a break at the connection between the ribbon riveting and the fuze. According to the physical structure of the submunition and the trajectory into which it was ejected, we analyzed the forces of the submunition in flight, deduced the related mathematical models, and clarify the key elements of the mechanics. In this paper, the commercial simulation software was used to calculate the mechanical properties of the ribbon. And the variation regularity between drop velocity and straightening force of ribbon are revealed. And the response characteristics of different material ribbon with different sizes of riveting holes and riveting joints under tensile action were simulated. The simulation results show that, in the trajectory environment with 30 m/s~55 m/s typical stream speed, the tensile force of the ribbon is less than 300 N, and the application concentration of the connecting parts of the riveting joint and the ribbon will not cause the failure of the kevlar ribbon, but it will cause the failure of the nylon ribbon. In order to verify the variation of the tension of kevlar ribbons in different trajectory environments, we designed the experimental scheme of tension test of the ribbon straightening section of submunition and conducted experiments. Experimental results and numerical simulation results revealed the same law. This paper provides effective technical support for solving the problem of unexploded submunitions.

1. Introduction

1.1. Background. The humanitarian damage caused by the unexploded submunitions is one of the hot issues of concern to the international community at present. Currently, cluster munitions equipped by various countries are mainly dual-purpose submunitions, which are referred to as submunitions in the following [1, 2]. This type of submunition is small in volume, mostly using flexible ribbon as stabilizing devices for submunition, while the ribbon also acts as part of a fuze. Therefore, the design of ribbon occupies a very important position in designing submunition.

It was found that a large number of unexploded submunitions which was caused by a break at the connection between ribbons and the fuzes in the post-war cleaning-up of the battlefield and shooting range experiments [3]. Figure 1 shows a typical submunition. Figure 2 shows the unexploded submunition. It can be seen from Figure 2 that the connecting part of the ribbon and fuze was broken and the ribbon falls off, resulting in the production of unexploded submunitions.

The phenomenon shown in Figure 2 may occur in straightening sections where the ribbon is the most stressed. Therefore, it is necessary to conduct a thorough study on the mechanical properties of the submunition's ribbon straightening section. There are three sections after submunitions that were ejected from the cluster munitions, that is, projectile, straightening, and deceleration section. Projectile

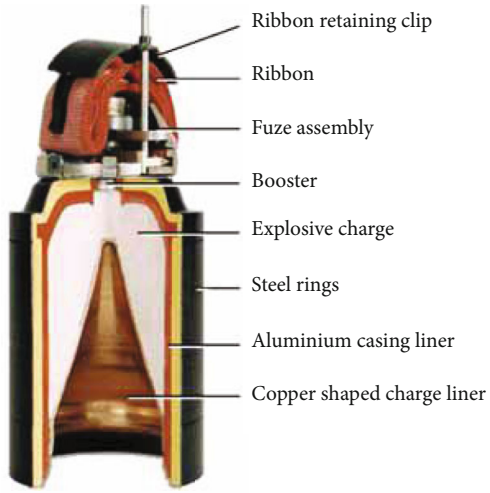

Figure 1: Typical submunition [3].

is the process of the submunition that separates from the ammunition until the ribbon begins to pull out. This segment provides initial conditions for the straightening segment. Straightening refers to the process of the beginning of the ribbon stretches out to the straight. The deceleration section refers to the submunition slowing down continuously which is caused by the air resistance generated by straightening.

The literature [4] introduced a new disk-ribbon supersonic parachute and its application to supersonic dispersed flat-faced submunition. The literature [5] investigated ribbons, parafoils, and loop systems and considered the drag and flapping characteristics of aerodynamic decelerators in a low-speed flow about these systems. The literature [6] carried out CFD simulations of flat-faced submunition with disk-ribbon parachute were based on multiblock structured grids. The literature [7] explored numerical simulation on single projectile and projectile with ribbon-parachute based on the validation of wind tunnel experiment. The literature [8] summarized the aerodynamic results from these tests (in particular the drag characteristics) and discussed the recent program developments. The literature [9] conducted an extensive experimental program to determine the aerodynamic characteristics of grenade ribbon stabilizers.

In summary, it can be seen that the relevant literature mainly focuses on the study of the aerodynamic characteristics of the ribbon, and less attention is paid to the material of the ribbon and the stress concentration phenomenon of the riveting part of the ribbon. Through mechanical modeling, numerical calculation, and laboratory experiments, it is explained that the use of kevlar materials in the ribbon can meet the technical needs of submunition. The stress concentration of the connecting parts of riveting joints and ribbons will not cause the failure of the kevlar ribbon but will cause the failure of the nylon ribbon.

1.2. This Article's Work and Contribution

(1) Based on the physical structure of the submunition and the trajectory environment into which it was ejected, we analyze the force on the submunition and ribbon in flight, deduce the related mathematical model, and clarify the key elements of the mechanics

(2) In this paper, the commercial simulation software was used to calculate the pull of the ribbon. And the variation regularity between drop velocity and straightening force of the ribbon was revealed. And the response characteristics of different material ribbons with different sizes of riveting holes and riveting joints under tensile action were revealed

(3) In order to verify the variation of the tension of kevlar ribbons in different trajectory environments, we designed the experimental scheme of tension test of the ribbon straightening section of submunitions and conducted experiments. Experimental results and numerical simulation results revealed the same law

2. Mechanical Model of the Submunition's Ribbon Straightening Section

2.1. The Physical Structure of a Submunition. The ribbon is used as a stabilizer for the submunition, and its model is shown in Figure 3, which mainly includes the body, fuze, and ribbon. The head of the submunition is a cylinder, and there is a flat-concave cylindrical hole at the edge of the head. The unstable turning moment of the submunition decreases with the ribbon on the tail. The shorter and narrowed the ribbon, the more stable the submunition. The ribbon is made of nylon, which is easy to fold and fill into the submunition. The quality of being flexible is smaller than that of metal, which allows the center of gravity of submunition to move forward, which is good for the distribution of the submunition.

2.2. Forces on the Submunition and Ribbon

2.2.1. Force Analysis

(1) Air resistance

$$R_x = \frac{1}{2}\rho v_r^2 S C_{x,} \tag{1}$$

where R_x is air resistance; ρ is air density; v_r is relative velocity; S is the maximum cross-sectional area of the submunition body; and C_x is drag coefficient.

To study the resistance of the various parts of the submunition, the air resistance coefficient of the submunition is expressed as

$$C_x = C_{xd} + C_{xs}, \tag{2}$$

where C_{xd} is the air resistance coefficient of the body and C_{xs} is the air resistance coefficient of the ribbon.

Figure 2: The unexploded submunition whose ribbon falls off [3].

(2) Lift

$$R_y = \frac{1}{2}\rho v_r^2 S C_y, \tag{3}$$

where R_y is lift and C_y is lift coefficient.

The body lift forms the turning moment.

(3) Magnus force

$$R_z = \frac{1}{2}\rho S d \dot{\gamma} v_r C_z'' \delta_r, \tag{4}$$

where R_z is Magnus force; d is body diameter; $\dot{\gamma}$ is angular acceleration along the longitudinal axis; C_z'' is the derivatives of the Magnus force coefficient; and δ_r is the relative attack angle.

Rotating submunitions fly at a high angle of attack producing a Magnus force. Generally, the Magnus force is only a few percent of the lift and has less impact on the movement of the submunition.

(4) Gravity

Gravity along the y coordinate axis of the earth's coordinate system, that is

$$\begin{bmatrix} G_x \\ G_y \\ G_z \end{bmatrix} = \begin{bmatrix} 0 \\ -mg \\ 0 \end{bmatrix}. \tag{5}$$

2.2.2. Moments Analysis

(1) Pitching moment

$$M_z = \frac{1}{2}\rho S l v_r^2 m_z, \tag{6}$$

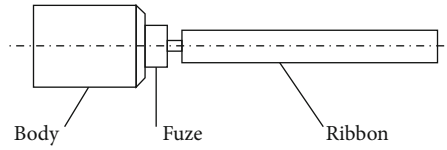

Figure 3: The structure of a submunition.

where M_z is pitching moment and m_z is pitch moment coefficient.

For convenience, the static moment is divided into two parts, the stable moment and the overturning moment.

M_{z1} is the stable moment and M_{z2} is the overturning moment.

The stable moment comes from a drag on the ribbon. The overturning moment is from the lift on the body.

(2) Extreme damping moment

$$M_{xd} = \frac{1}{2}\rho v^2 S l m_{xd}, \tag{7}$$

where M_{xd} is extreme damping moment; m_{xd} is extreme damping moment coefficient; m_{xd}' is the derivative of the extreme damping moment; and l is body length (does not include the ribbon's length).

2.3. Analysis of the Force on the Ribbon. From an aerodynamic point of view, there are three characteristics of the force on a ribbon.

The aerodynamic action point acting on the ribbon does not change with time, speed, and flight attitude, and the action point is always at the point where the ribbon and fuze are connected.

The direction of the aerodynamic composition of forces acting on the ribbon does not change with time, speed, and flight attitude. It always flies in the opposite direction of the submunition but at the same line with the speed vector.

The aerodynamic composition of forces acting on the ribbon includes only drag but not lift. It is because when the

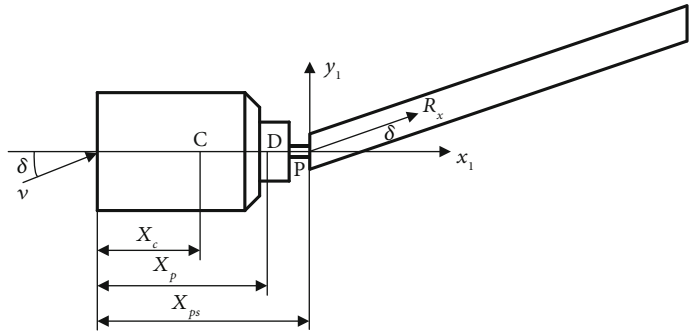

Figure 4: Analysis of the force on the ribbon.

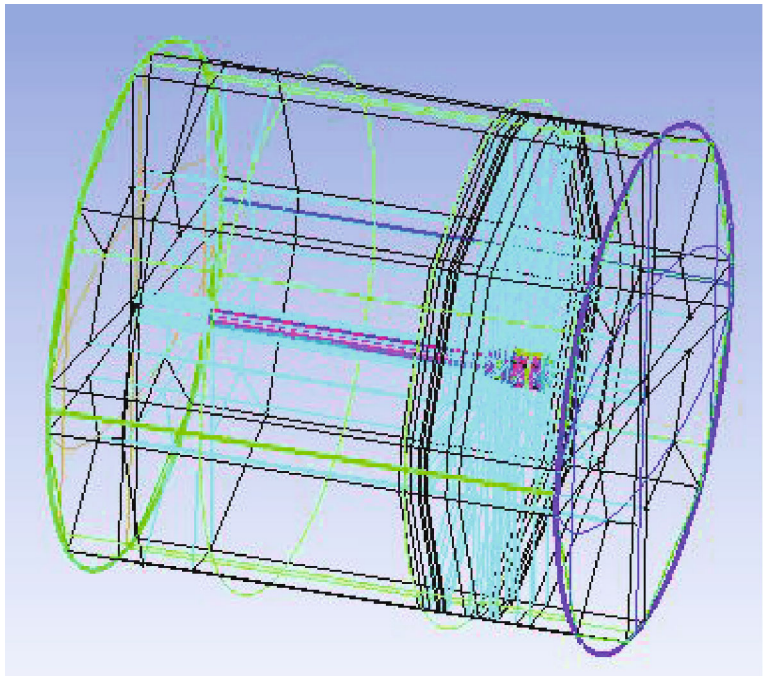

Figure 5: The line graph of submunition's blocking.

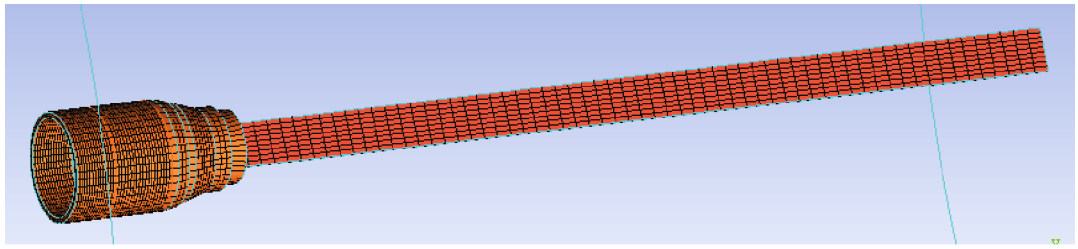

Figure 6: Three-dimensional grid of the submunition.

submunition causes an angle of attack, there is a pressure difference between the upper surface and the lower surface of the ribbon. However, the ribbon is flexible, it can deflect freely to a place where the pressure is low until the pressure balance between the upper surface and lower surface of the ribbon, that is, the direction of the ribbon is same with speed and the pressure difference is zero which means there is no lift. We can see that the ribbon is stable by the drag.

The drag on the ribbon can be decomposed into two components. When the drag R_x is projected on the axis of the projectile, it is called the axial force X_1 and $X_1 = R_x \cos \delta$. When the drag is projected perpendicularly to the axis of the projectile, it is named the normal force Y_1 and $Y_1 = R_x \sin \delta$. This is shown in Figure 4.

The dimensionless coefficients of the axial force X_1 and the normal force Y_1.

The axial force coefficient is $C_{X_1S} = C_{XS} \cos \delta$.

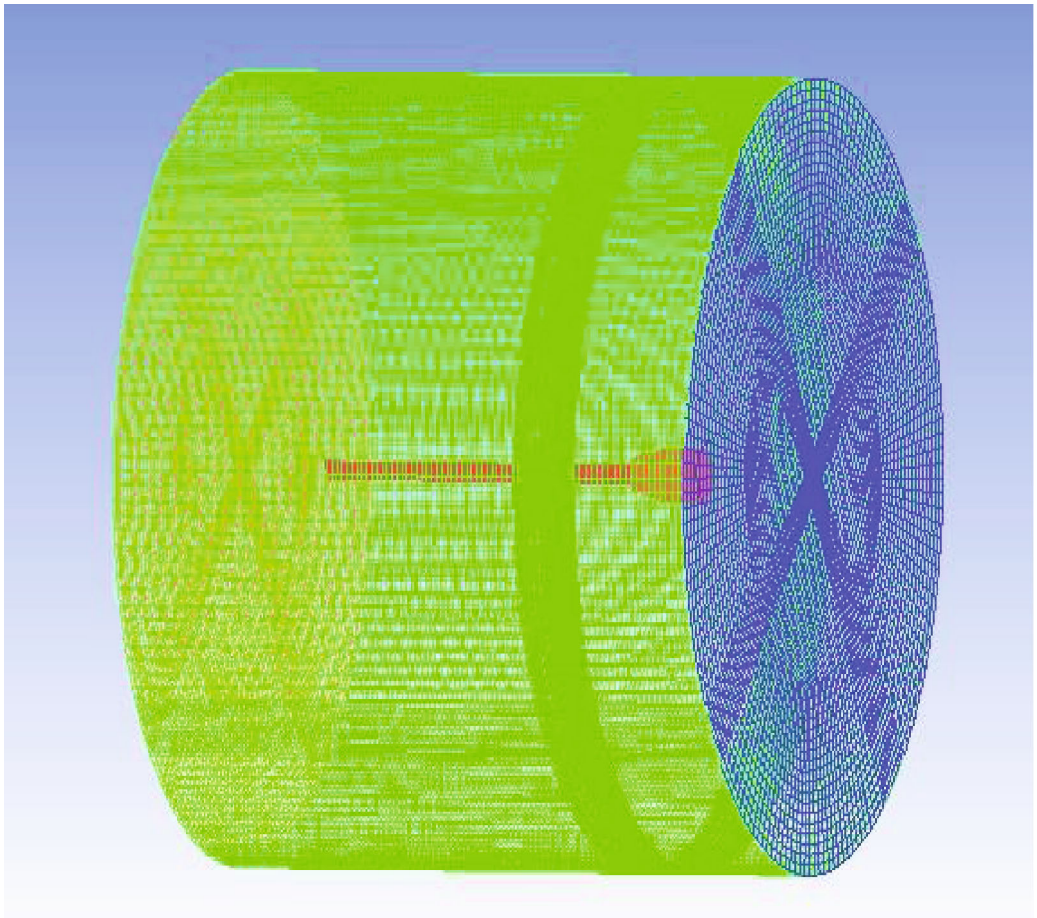

Figure 7: The three-dimensional computation grid of outflow field of the submunition.

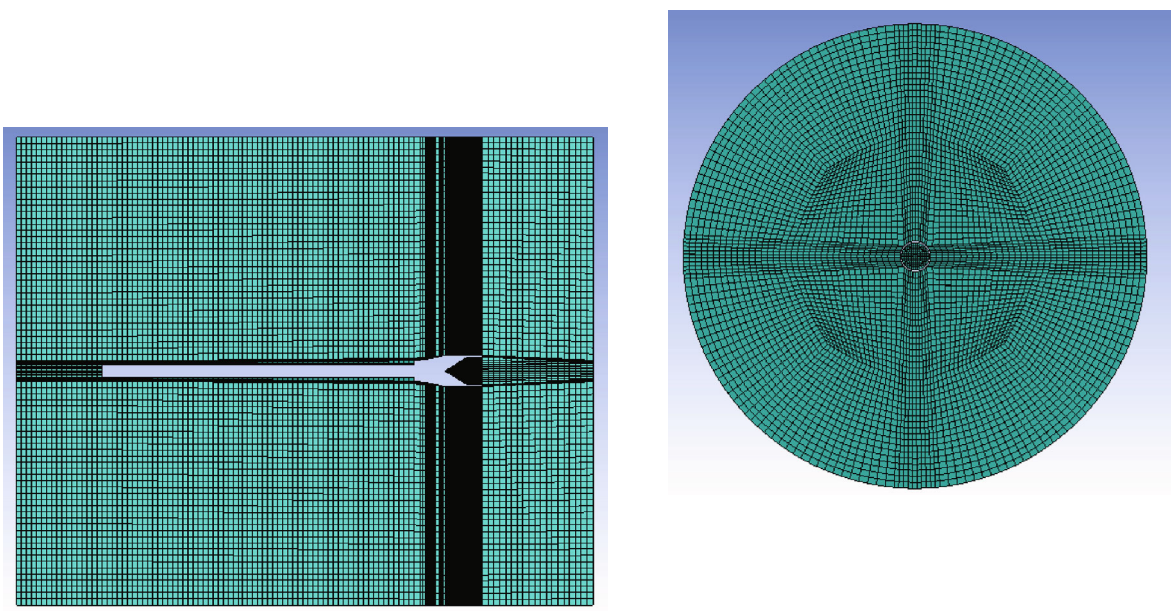

(a) The vertical section of the computation grid

(b) The cross-section of the computation grid

Figure 8: The section of outflow field calculation grid.

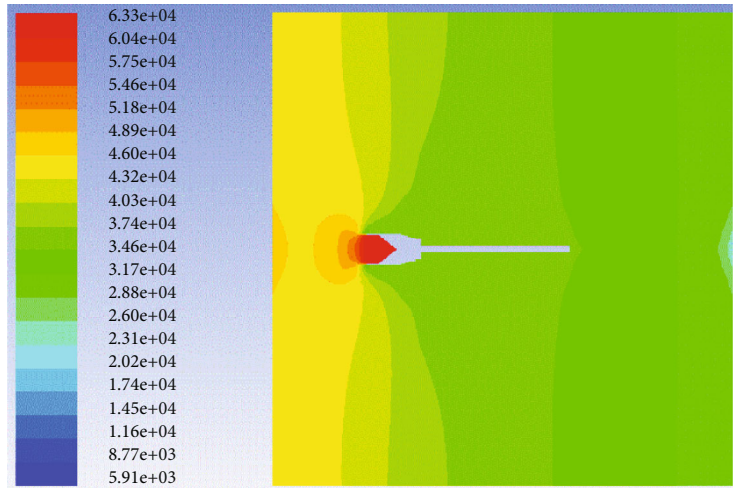

Figure 9: Pressure contour when $v = 30m/s$, $\alpha = 0^{\circ}$.

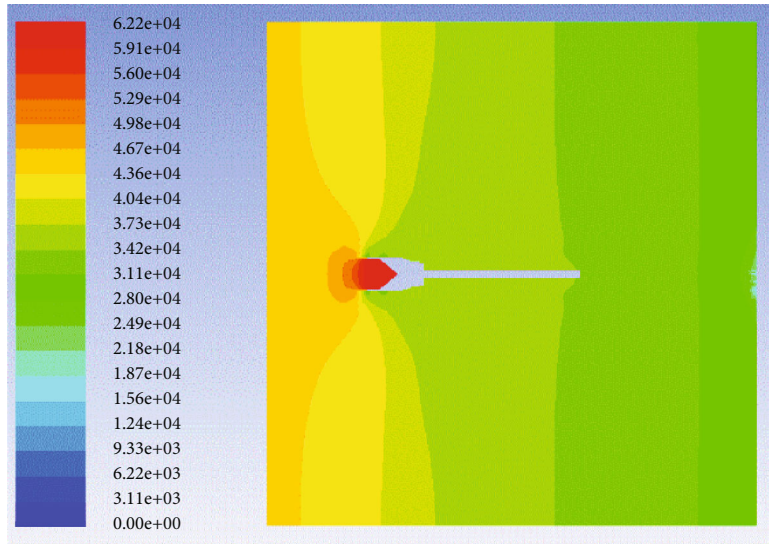

Figure 10: Pressure contour when $v = 35m/s$, $\alpha = 0^{\circ}$.

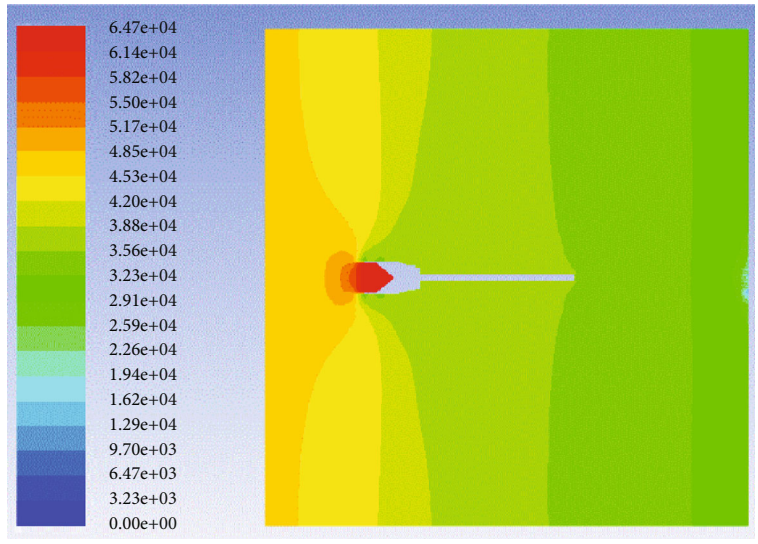

Figure 11: Pressure contour when $v = 40m/s$, $\alpha = 0^{\circ}$.

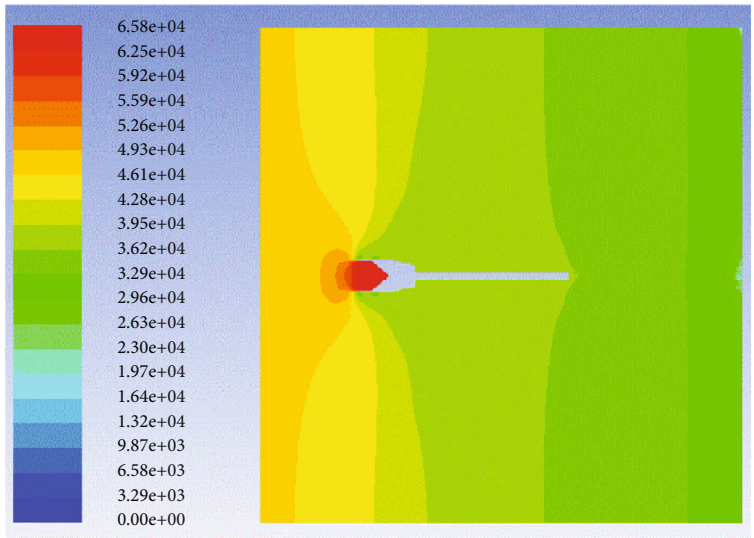

Figure 12: Pressure contour when $v = 45m/s$, $\alpha = 0^{\circ}$.

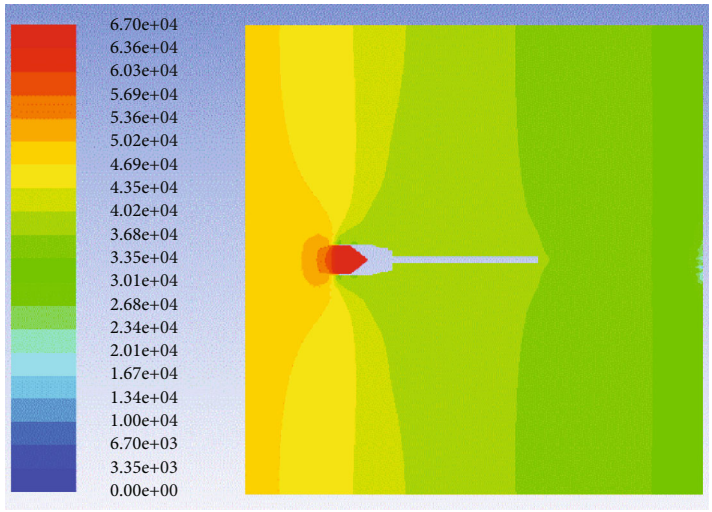

Figure 13: Pressure contour when $v = 50m/s$, $\alpha = 0^{\circ}$.

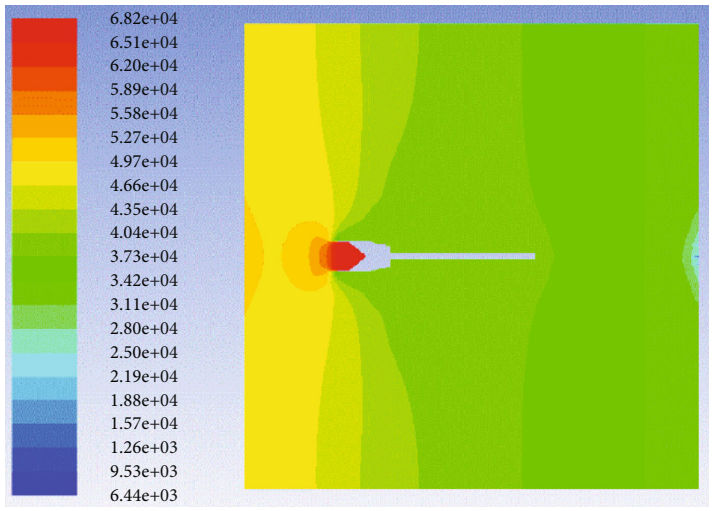

Figure 14: Pressure contour when $v = 55m/s$, $\alpha = 0^{\circ}$.

Table 1: The pull on the ribbon under different speeds.

To flow speed (m/s)	Stretch of the tension (N)
30	137.2
35	163.0
40	194.1
45	229.2
50	267.8
55	299.7

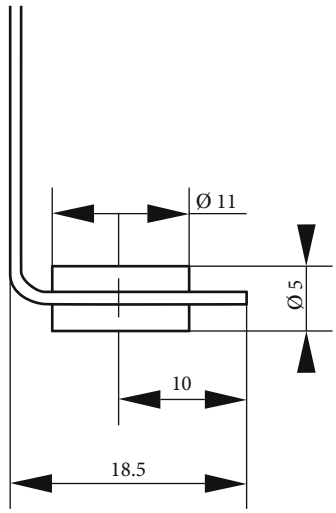

Figure 15: An installation dimension diagram of specimens.

The normal force coefficient is $C_{Y_1S} = C_{YS} \sin \delta$.

In the formula, C_{xs} is the drag coefficient of the ribbon and δ is the angle of attack.

The drag coefficient of the ribbon is

$$C_{XS} = \frac{R_{XS}}{1/2\rho V^2 S}. \tag{8}$$

In the formula, R_{XS} is the total drag of ribbon.

The moment coefficient of ribbon is $m_{zs} = C_{Y_1S} X_{ps}$ (The reference point of m_{zs} is the head of the submunition).

$$\bar{X}_{ps} = X_{ps}/l. \tag{9}$$

In the formula, $\bar{X}_{ps}$, is the distance between the action point of drag on the ribbon resistance point P and the vertex of the warhead.

From the above analysis, we can see that if we know the drag R_{XS} on the ribbon, other aerodynamic forces such as axial force, normal force, and the stable moment can be calculated.

3. Numeral Calculations

3.1. The Basic Control Equations of Fluid Dynamics. In this paper, we base our numerical calculations on the laws of mass, momentum, and energy conservation. The control equations are mathematical descriptions of these conservation laws.

Table 2: The working condition of the riveting hole of the ribbon.

Working conditions	Working conditions (1)	Working conditions (2)	Working conditions (3)
Hole diameter (mm)	3	4	5

The flow field characteristics of the submunition stabilization device can be analyzed with the N-S equation. Because of the small drop rate of submunition, air can be defined as incompressible, so the energy equation cannot be solved. Air physical parameters take constant values. The governing equations are as follows:

$$\frac{\partial}{\partial x_i}(\rho u_i) = 0, \tag{10}$$

$$\frac{\partial}{\partial x_i}(u_i u_j) = -\frac{1}{\rho}\left(\frac{\partial p}{\partial x_i} + \frac{\partial \tau_{ij}}{\partial x_j}\right) + g_i. \tag{11}$$

In the formula, u_{ij} is velocity of flow p is static pressure, ρ is density, τ_{ij} is stress tensor, and g_i is Gravity volume force in i direction; stress tensor is given by the following formula.

$$\tau_{ij} = \left[\mu\left(\frac{\partial u_i}{\partial x_i} + \frac{\partial u_j}{\partial x_i}\right)\right] - \frac{2}{3}\mu\frac{\partial u_1}{\partial x_1}\delta_{ij}, \tag{12}$$

where δ_{ij} is viscosity.

3.2. Boundary Conditions. The main boundary conditions involved in the numerical simulation are inlet boundary conditions and exit boundary conditions.

3.2.1. Inlet Boundary Conditions. In this paper, the free-flow Mach number and static parameters are set. As the pressure far-field boundary conditions require that the density be calculated using the ideal gas law, we must calculate the far inlet boundary.

3.2.2. Outlet Boundary Conditions. Since the submunition are only in subsonic flow conditions, we set the static pressure at the flow field's outlet boundary as the pressure outlet boundary condition.

In order to simulate the infinite flow field and study the flow around the submunition, a cylindrical calculation domain is established. The calculation domain selection. The distance between the front cross-section and the warhead is 5 times the length of the submunition's radius. The distance between the behind cross-section and the cross-section of the ribbon's tail is 5 times the length of the submunition's radius. The vertical distance between the outer boundary and the body is 10 times the length of the radius. The outer flow field surrounding the projectile is divided into several blocks; then, the O-Block is generated.

Table 3: Nylon material parameters.

Density ρ (kg/m^3)	Elastic modulus, E (GPa)	Poisson-pine ratio, ν	Fracture strain	Tangent modulus (MPa)	Yield strength (MPa)
1140	2.83	0.4	0.6	14	80

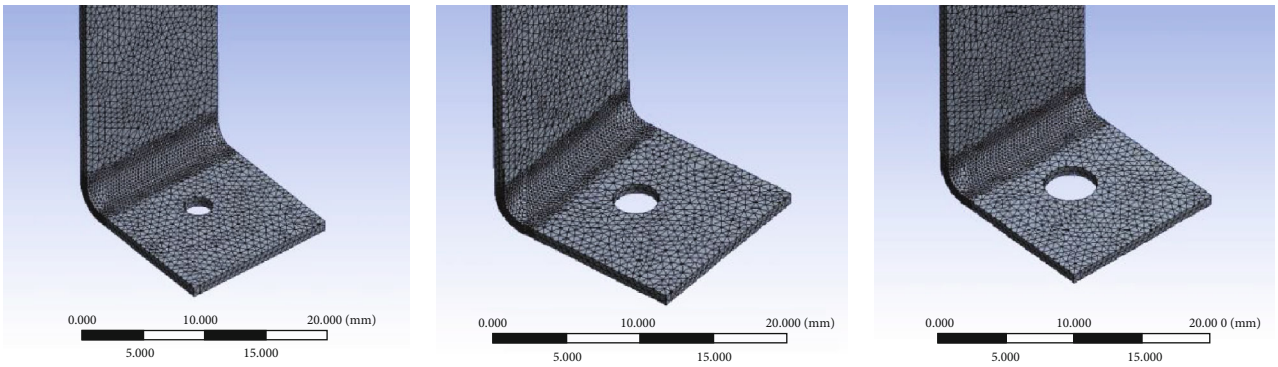

(a) Working conditions (1) (b) Working conditions (2) (c) Working conditions (3)

Figure 16: Three finite element model of riveting hole opening condition (fixed bolt hiding).

Table 4: The critical tensile force of nylon ribbon corresponding.

Working conditions	Working conditions (1)	Working conditions (2)	Working conditions (3)
Critical tensile force (N)	47	46.8	47.5

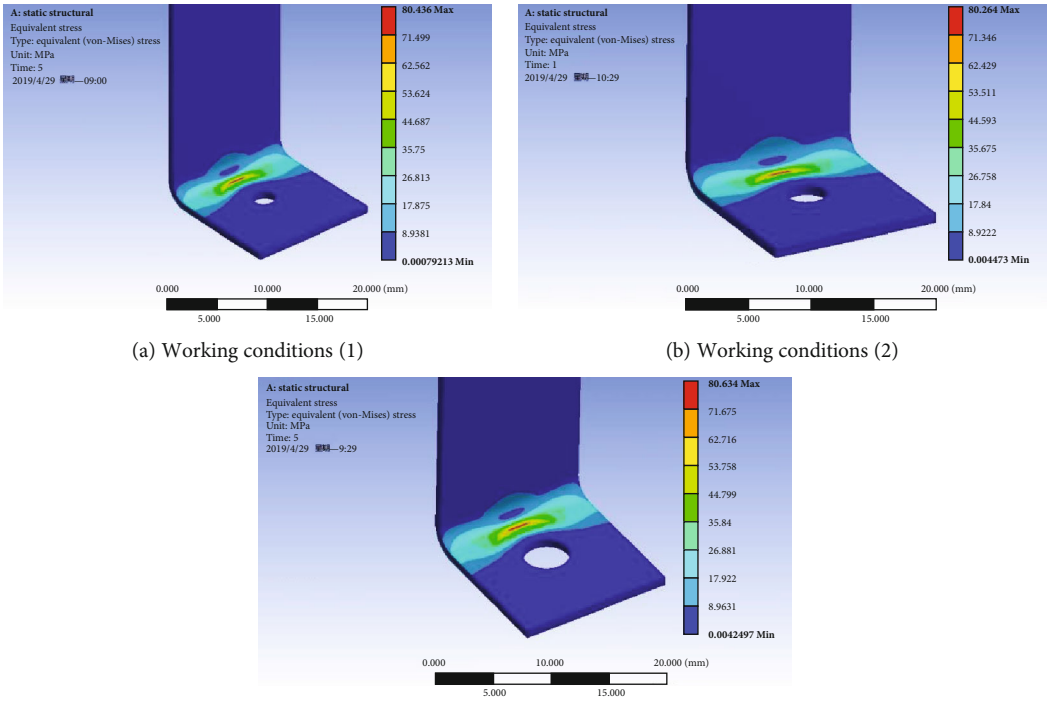

(a) Working conditions (1) (b) Working conditions (2)

(c) Working conditions (3)

Figure 17: Stress cloud map corresponding to the change of the opening diameter of nylon ribbon.

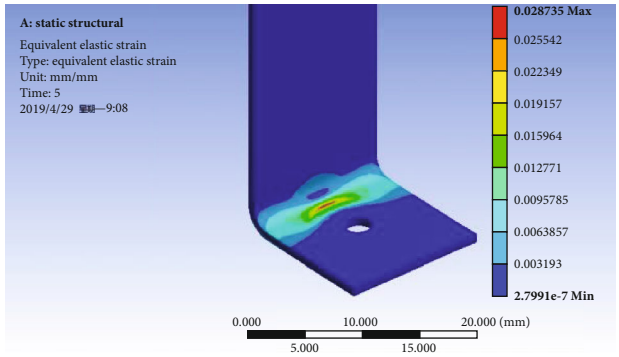

(a) Working conditions (1)

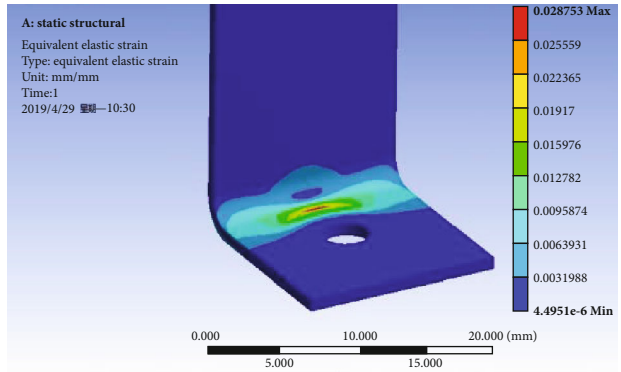

(b) Working conditions (2)

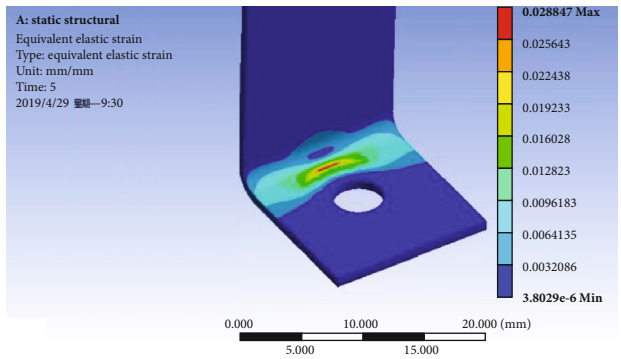

(c) Working conditions (3)

Figure 18: Strain cloud diagram corresponding to the change of the opening diameter of nylon ribbon.

As is shown in Figure 5, it is used to simulate the flow in the boundary layer.

3.3. Mesh. The submunition studied in this paper is composed of plat concave warheads, cylinder shells, and ribbons. Refine grid where shock and expansion waves may occur. The three-dimensional grid of submunition is shown in Figure 6. The three-dimensional computation grid of the outflow field of the submunition is shown in Figure 7. The vertical section and the cross-section are shown in Figure 8. We can see that the boundary layer has been refined.

3.4. The Characteristics of the Flow Field. In this paper, there are 6 kinds of conditions. The diameter of the body is 42.5 mm. The ribbon' size is 17 mm × 340 mm × 1 mm. The angle of attack is 0° and the flow rate is 30 m/s, 35 m/s, 40 m/s, 45 m/s, 50 m/s, and 55 m/s, respectively. From Figures 9–14, we can see the pressure contour for the outflow field of submunition in different conditions, which are calculated by numerical simulation. The vertical axis is the pull force, and the horizontal axis is the incoming velocity from Figures 9–14. As can be seen from Figures 9–14, when the submunition is flying at low speed, the incoming flow is compressed in the concave surface of the body and the local pressure increases rapidly. As the incoming flow passes from the concave surface through the body, the airflow expands and the pressure drops rapidly. Due to the air viscosity, the Mach number on the cylinder surface is low and the pressure

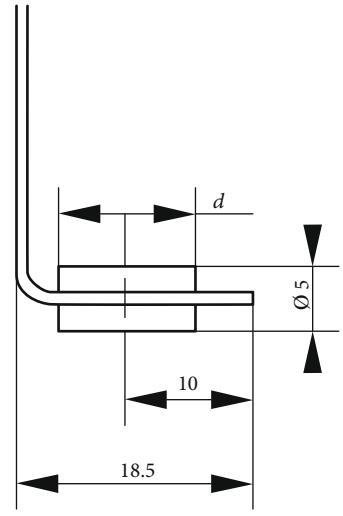

Figure 19: An installation dimension diagram of riveting joint.

increases. Because the ribbon is a flexible, the upper and lower surfaces' pressure adjust automatically to keep balance, but also because the angle of attack is 0°, the pressure contours are symmetrical.

The drag on the ribbon under different speeds is shown in Table 1. It can be seen from Table 1 that the pull on the connection between the ribbon and the submunition is different when the incoming flow's velocity is different. The higher the flow's velocity is, the larger the pull is. The

Table 5: Diameter working conditions of riveting joints.

Working conditions	Working conditions (A)	Working conditions (B)	Working conditions (C)
Riveting connector diameter (mm)	7	9	11

Table 6: The critical tensile force of nylon ribbon corresponding to different riveting joint diameters.

Working conditions	Working conditions (A)	Working conditions (B)	Working conditions (C)
Critical tensile force (N)	41	41.5	46.8

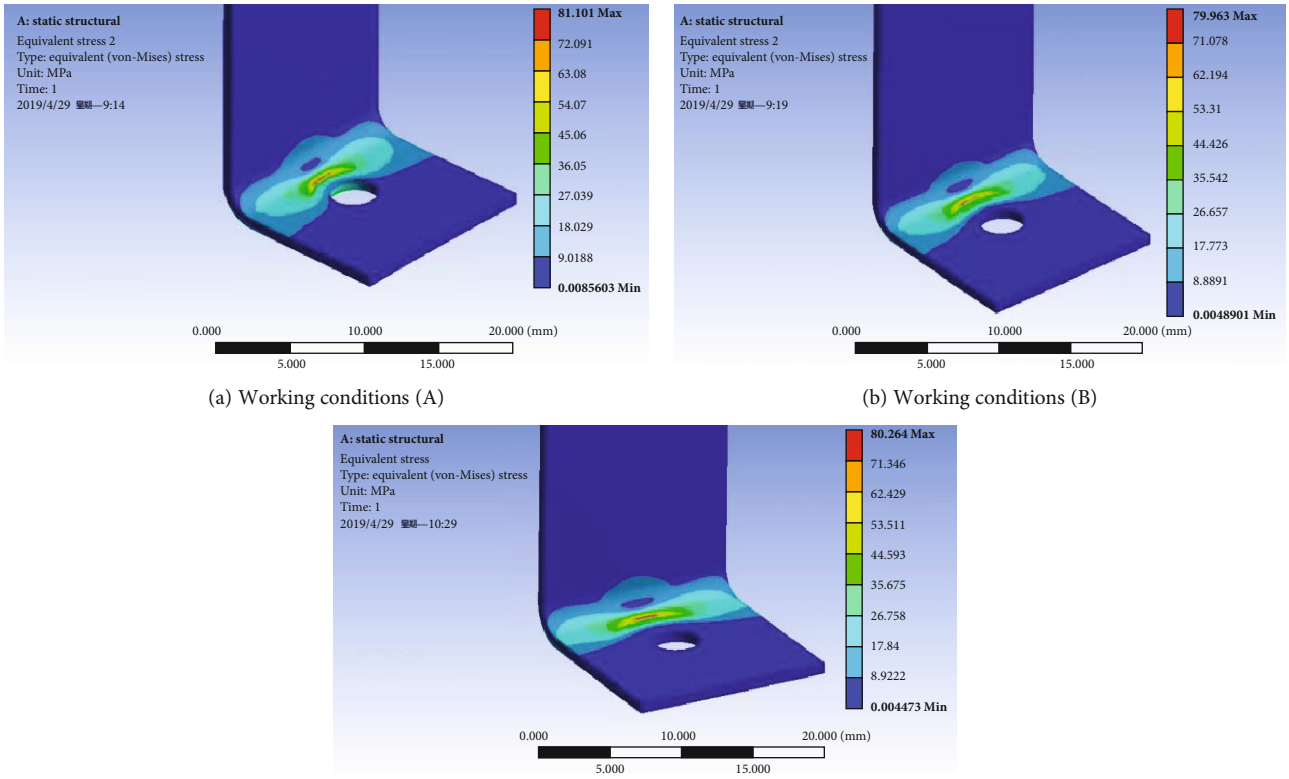

(a) Working conditions (A)

(b) Working conditions (B)

(c) Working conditions (C)

Figure 20: Stress cloud map corresponding to the change of diameter of the riveting joint in nylon ribbon.

simulation results show that when the incoming flow's velocity is 30 m/s~55 m/s, the maximum pull on the ribbon is 299.7 N.

3.5. Simulation of Weak Parts of the Ribbon When It Is Pulled by the Tension. The mechanical characteristics of weak parts, that is, the ribbon and the riveting part of submunition were further analyzed. In this paper, the stress of the ribbon of nylon and kevlar materials, the riveting holes, and riveting joints with different sizes are simulated and analyzed and simplified during simulation, which mainly considers the function of the tensile force of ribbon tension.

3.5.1. Nylon Ribbon. Under the condition that the end distance of the riveting opening center is certain (the dimension relation is Figure 15), the diameter of the opening hole on the ribbon is changed, and the tensile strength of the ribbon is simulated and analyzed. The specific operating conditions are set as shown in Table 2, and the parameters of the levant materials are set in Table 3.

The tetrahedron unit grid is used in the simulation analysis. Because of the large curvature of this simulation model, the mesh partitioning method based on the patch conforming algorithm is adopted, and the local mesh of bending surface is refined, and three finite element models of working conditions are generated, as shown in Figure 16.

The yield strength of nylon material is 80 MPa, and by changing the stimulation parameters, it is found that the nylon material has local yield when the critical tensile force is set to values in Table 4. In three kinds of working conditions under the action of critical tensile force, the corresponding stress and strain cloud diagram is shown in Figures 17 and 18. Figures 17 and 18 show that the riveting hole diameter is not the same and the effect of the stress change of the bending part of the ribbon is not significant.

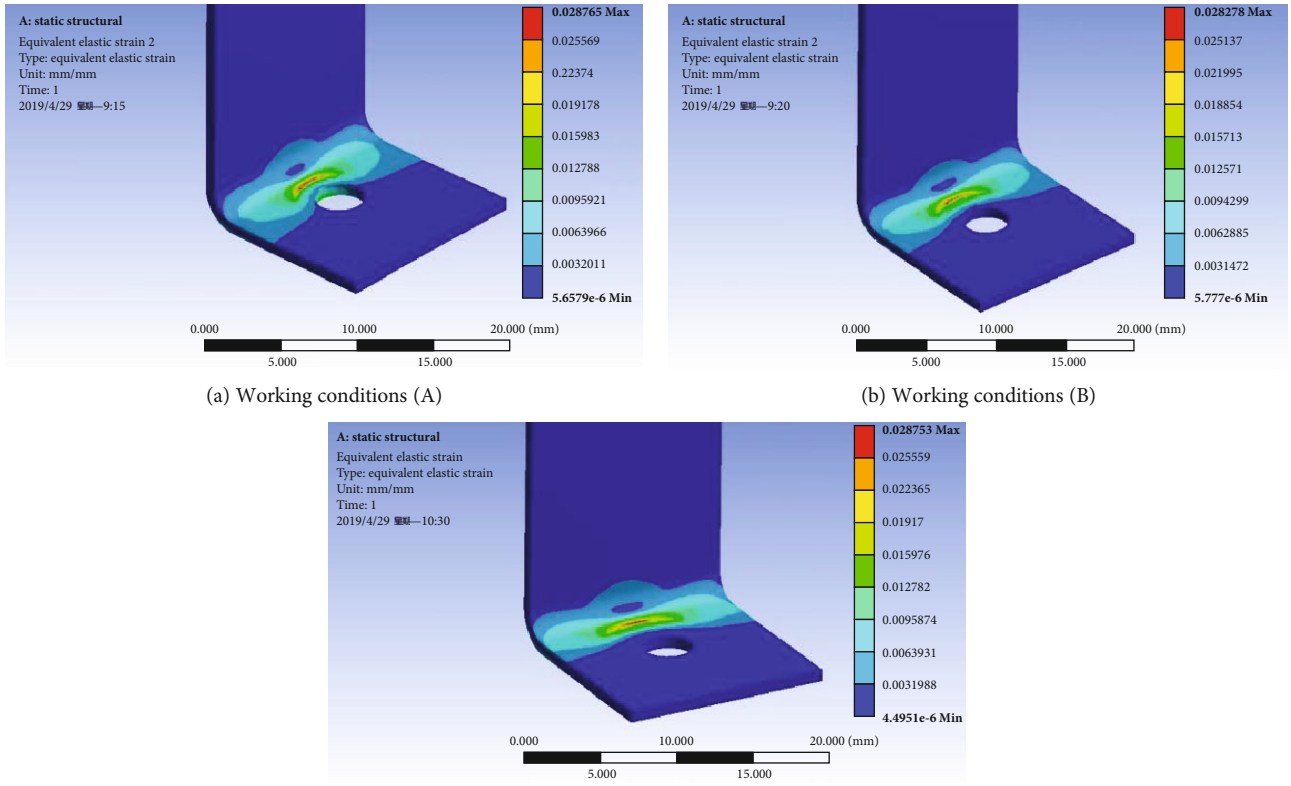

(a) Working conditions (A)

(b) Working conditions (B)

(c) Working conditions (C)

Figure 21: Strain cloud map corresponding to the change of diameter of the riveting joint in nylon ribbon.

Table 7: Kevlar ribbon parameters.

Xdirection elastic modulus, E_1 (GPa)	Y, Z direction elastic modulus, E_2, E_3 (GPa)	Y_z plane shear modulus, G_{23} (GPa)	X_y, X_z plane shear modulus, G_{12}, G_{13} (GPa)	Y_z plane Poisson's ratio, ν_{23}	X_y, X_z plane Poisson's ratio, ν_{12}, ν_{13}	Failure stress (GPa)
84.62	1.34	0.54	24.4	0.24	0.6	3.5

Table 8: The critical tensile force of kevlar corresponding to the working conditions of different opening diameters.

Working conditions	Working conditions (1)	Working conditions (2)	Working conditions (3)
Critical tensile force (N)	525	510	520

Because of the contact between the riveting joint and the ribbon, the change of the size of the riveting joint may lead to the change of the local force of the ribbon to a certain extent, forming the stress concentration, so this paper carries on the numerical simulation to this kind of condition in three kinds of working conditions. In the opening diameter size $D =$ 4 MM, the center distance from the vertical end of the ribbon is certain (size relationship as shown in Figure 19) and there was a change in the size of the rivet joint diameter; detailed working conditions are shown in Table 5.

The yield strength of nylon material is 80 MPa, and the nylon material has local yield when set to the critical tensile force values of Table 6 by simulation analysis. In three kinds of working conditions under the action of critical tensile force, the corresponding stress and strain cloud diagram is shown in Figures 20 and 21. Figures 20 and 21 shows that the diameter of riveting joints is not the same, and the contact point with riveting joints is easy to cause stress concentration phenomenon, so it is shown that the diameter of riveting joints needs to focus on.

3.5.2. Kevlar Ribbon. The simulation method is similar to that of nylon ribbon, the parameters of the kevlar ribbon are shown in Table 7, and the working condition setting is similar to that of the nylon ribbon. Table 8 shows the critical tensile force of the kevlar corresponding to the working conditions of different opening diameters.

Figure 22 shows a stress cloud map corresponding to the variation of the opening diameter of the kevlar ribbon. Figure 23 shows a strain cloud map corresponding to the variation of the opening diameter of the kevlar ribbon. Table 9 shows the critical tensile force of the kevlar ribbon corresponding to the diameter of different riveting joints. Figure 24 shows a stress cloud map corresponding to the

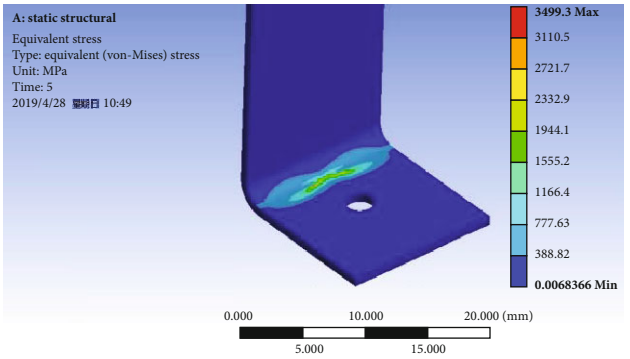

(a) Working conditions (1)

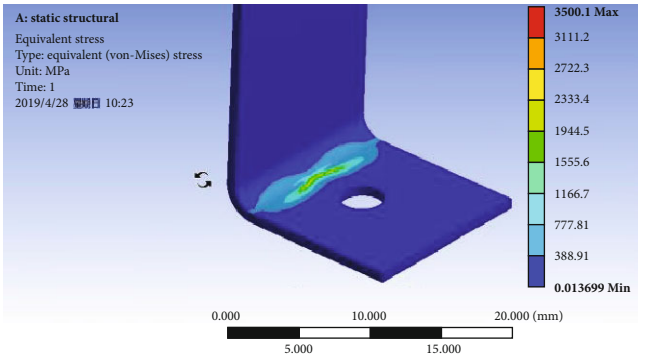

(b) Working conditions (2)

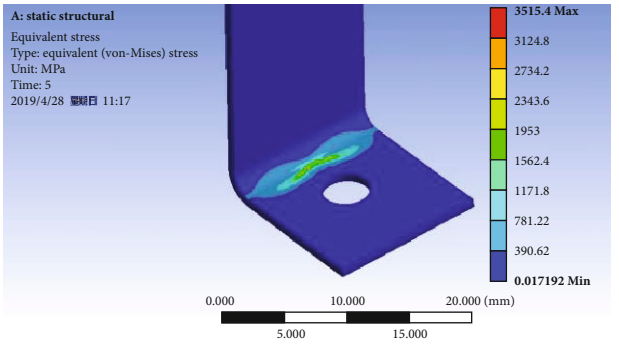

(c) Working conditions (3)

Figure 22: Stress cloud map corresponding to the change of the opening diameter of kevlar ribbon.

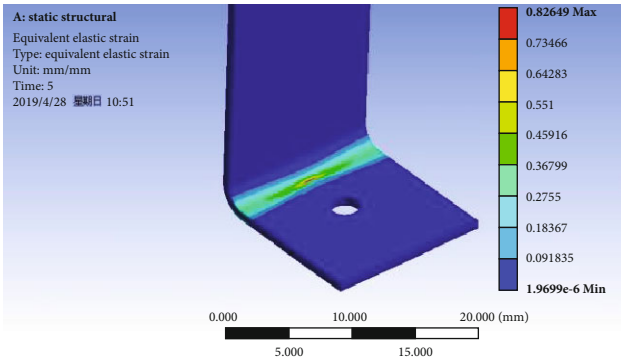

(a) Working conditions (1)

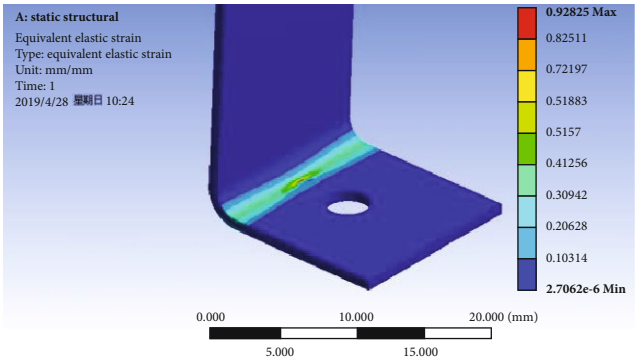

(b) Working conditions (2)

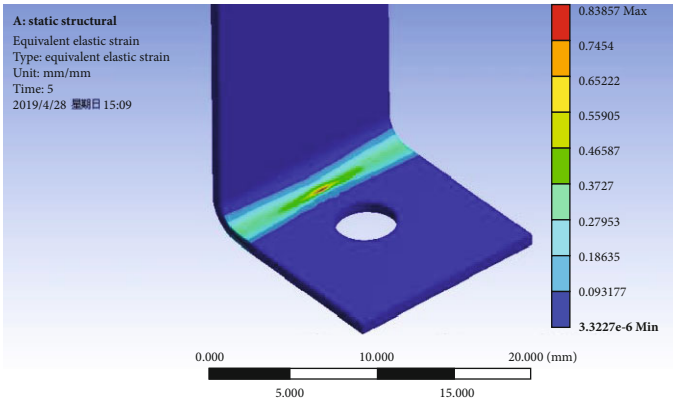

(c) Working conditions (3)

Figure 23: Strain cloud diagram corresponding to the change of the opening diameter of kevlar ribbon.

Table 9: The critical tensile force of the kevlar ribbon corresponding to the diameter of different riveting joints.

Working conditions	Working conditions (A)	Working conditions (B)	Working conditions (C)
Critical tensile force (N)	400	430	510

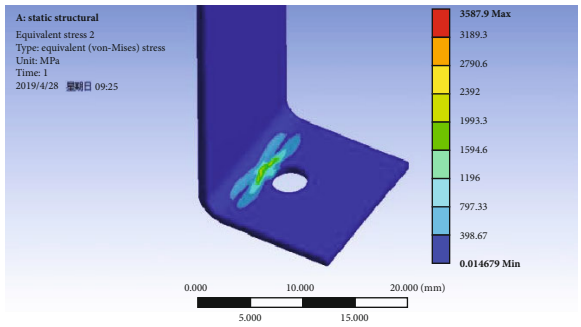

(a) Working conditions (A)

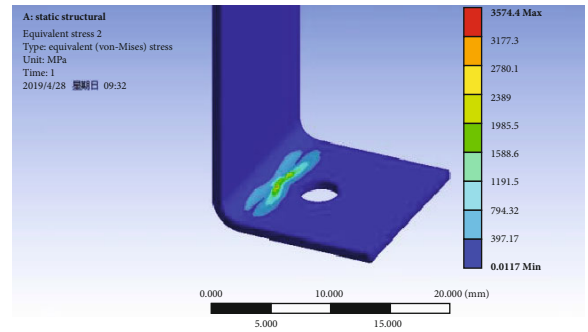

(b) Working conditions (B)

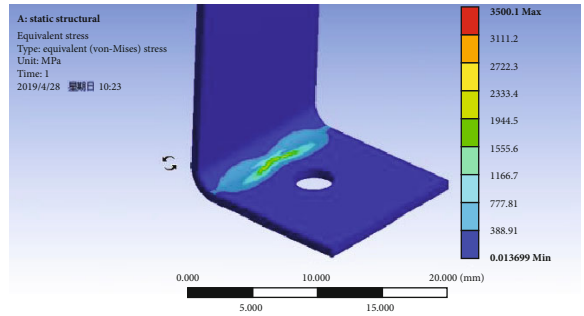

(c) Working conditions (C)

Figure 24: The stress cloud map corresponding to the change of the diameter of the riveting joint of the kevlar ribbon.

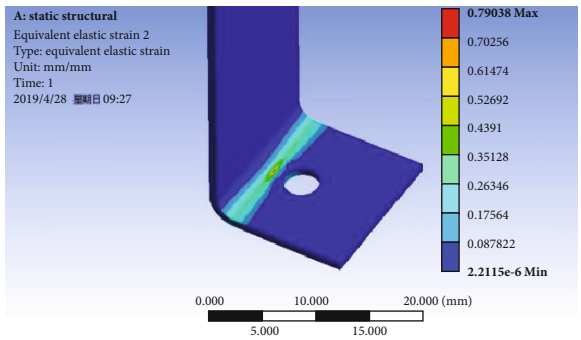

(a) Working conditions (A)

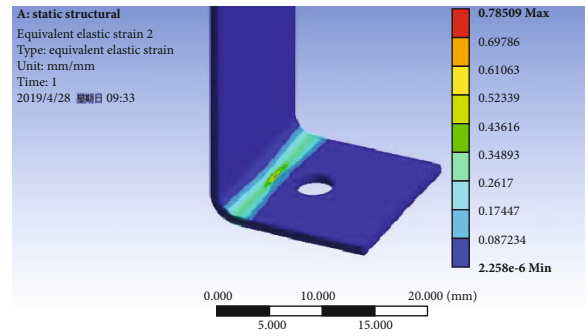

(b) Working conditions (B)

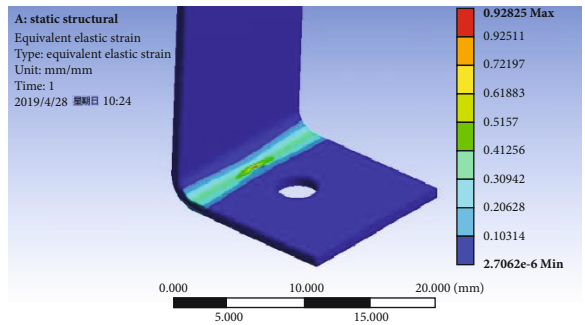

(c) Working conditions (C)

Figure 25: Strain cloud map corresponding to the change of the diameter of the riveting joint of kevlar ribbon.

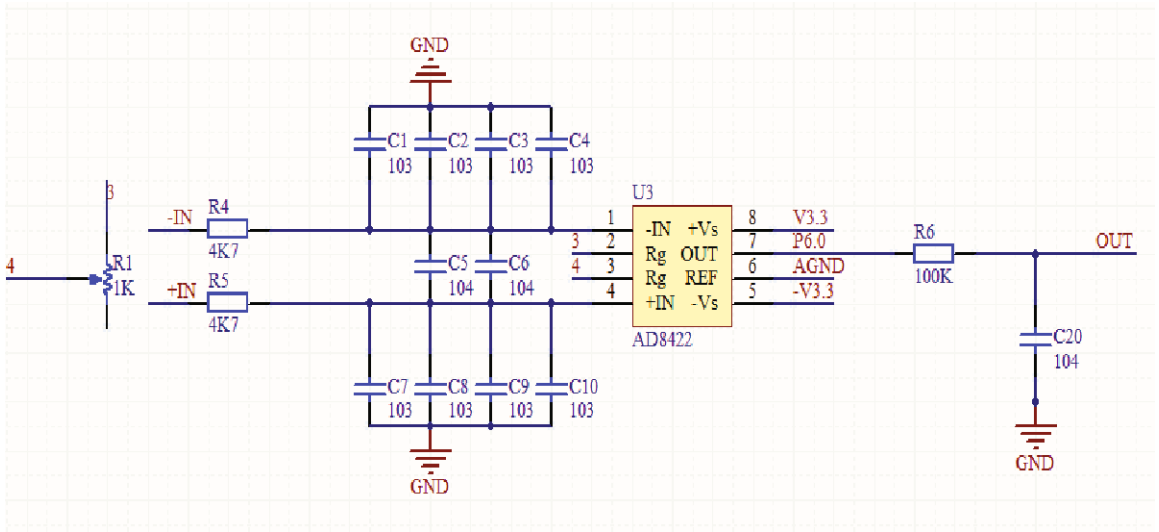

Figure 26: Signal conditioning circuit.

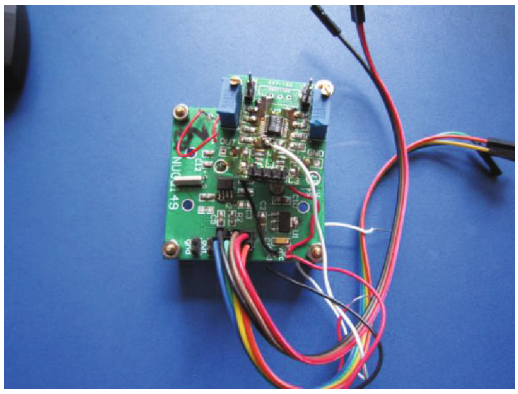

Figure 27: Test circuit board.

Figure 28: Experimental site.

Table 10: The experimental data of wind tunnel.

Wind speed (m/s)	First group	Second group	Third group	Fourth group	Fifth group	Average value (N)
30	135.2	135.0	135.5	135.9	136.0	135.52
35	161.3	159.5	160.1	162.3	159.1	160.46
40	191.0	190.8	191.5	191.3	192.6	191.44
45	224.4	223.5	225.1	225.3	223.8	224.42
50	263.4	263.2	263.1	263.8	263.9	263.48
55	293.5	293.6	293.1	293.8	299.1	294.62

Table 11: The calculated value and test value of the pull.

Wind speed (m/s)	The calculated value (N)	The test value (N)	Relative error
30	137.2	135.52	1.23%
35	163.0	160.46	1.59%
40	194.1	191.44	1.34%
45	229.2	224.42	2.01%
50	267.8	263.48	1.68%
55	299.7	294.62	1.78%

change of diameter of the riveting joint of the kevlar ribbon. Figure 25 shows a strain cloud map corresponding to the change of diameter of the riveting joint of the kevlar ribbon.

The following can be seen by simulating the weak link of the ribbon:

(1) The strength of the nylon ribbon is obviously insufficient, which is the main reason why submunitions give up the use of nylon ribbon

(2) The riveting part of the ribbon and the submunition is the weak link. The diameter of the riveting joint has a greater impact on the stress concentration than the riveting aperture. In the design, we need to pay

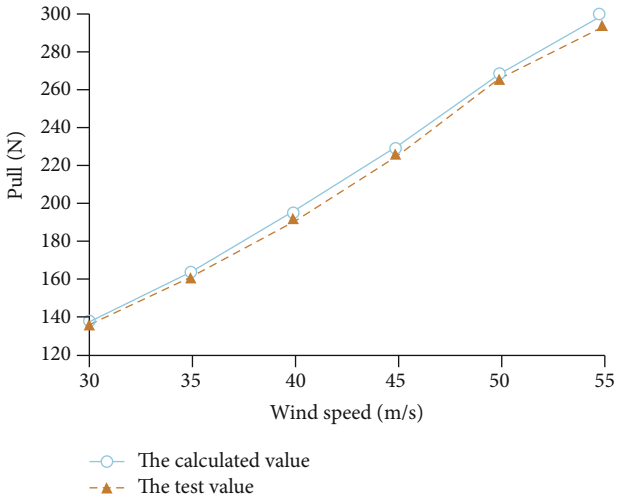

Figure 29: Calculated value and test value.

Figure 30: Tensile test.

attention to the matching between the diameter of the riveting joint and the features of the ribbon. The phenomenon of stress concentration is easier to form when the diameter of the riveting joint is small

4. Experimental Study

4.1. Experimental Program. The test system of the pull on the ribbon consists of three parts, sensors, signal conditioning circuits, and software. We use the internal and external thread tension sensor EVT-20TH produced by Shanghai You Ran Sensor Technology Company and adopt the AD8422 device produced by the United States ANALOG DEVICE company as the core chip of the signal conditioning circuit. The design of the signal conditioning circuit is shown in Figure 26. Figure 27 shows the test circuit board.

4.2. Wind Blow. We conducted a hairdryer experiment at the Xishan Laboratory of Beijing Institute of Technology. Figure 28 shows the experimental site. We connected the kevlar ribbon to the sensor and put it into a vertical wind tunnel for the blowing test to verify characteristics of the pull of the submunition's kevlar ribbons. The measured data is in

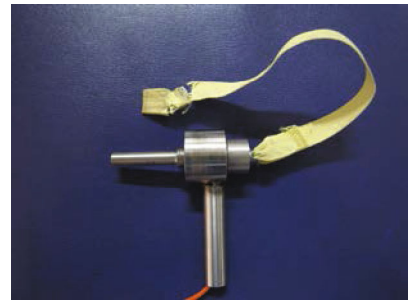

Figure 31: Ribbon break.

Table 10, and the calculated and test values are summarized in Table 11.

We used the calculated value of the pull of the ribbon and the test value of the wind tunnel experiment to establish the values shown in Figure 29. It can be seen from Figure 29 that the calculated value is slightly larger than the wind tunnel test value, but the overall trend is in a good agreement. Because of the error which affects the data collected by the sensor and the relative error is less than 5%.

In order to further verify the simulation conclusion, the test was carried out by using a tensile machine. When the test shows 500 N, and the kevlar ribbon was broken, and the experimental results were the same as the simulation result, the experimental results are shown in Figures 30 and 31.

5. Conclusion

According to the physical structure of the submunition and the trajectory into which it was ejected, we analyze the forces of the submunition in flight, deduce the related mathematical models, and clarify the key elements of the mechanics. In this paper, the commercial simulation software was used to calculate the mechanical properties of the ribbon. And the variation regularity between drop velocity and straightening force of the ribbon is revealed. And the response characteristics of different material ribbons with different sizes of riveting holes and riveting joints under tensile action were simulated. The simulation results show that in the trajectory environment with 30 m/s~55 m/s typical stream speed, the tensile force of the ribbon is less than 300 N, and the application concentration of the connecting parts of the riveting joint and the ribbon will not cause the failure of the kevlar ribbon, but it will cause the failure of the nylon ribbon. In order to verify the variation of the tension of kevlar ribbons in different trajectory environments, we designed the experimental scheme of tension test of the ribbon straightening section of submunition and conducted experiments. Experimental results and numerical simulation results revealed the same law.

Because the study of the mechanical characteristics of the pull straight segment of the submunition's ribbon is very difficult and the workload is very complicated, this paper only makes some preliminary attempts in combination with the theory and laboratory experiments. It should be noted that although the submunition's ribbon studied

in this paper can reflect its mechanical properties, there are some differences with the real parameters of the submunition's ribbon. The results of the study have a certain impact on the stress concentration values of the ribbon, but the quantitative analysis based on the method of this paper is meaningful. Next, the mechanical properties of the full trajectory of the submunition's ribbon will continue to be studied.

Data Availability

The data used to support the findings of this study are available from the corresponding author upon request.

Conflicts of Interest

The authors declare that they have no conflicts of interest.

Acknowledgments

This work was supported by the Focus on Research and Development Program (general) in Shanxi under grant 201603D121038, the Key Laboratory Open Research Fund Projects of NUC under grant DXMBJJ2017-10, the Key Laboratory Open Research Fund Projects of Advanced Manufacturing Technology Laboratory in Shanxi under grant XJZZ201704, and the Natural Science Foundation of Shanxi Province under grant 201801D221369.

References

[1] D.-z. Qin and N.-j. Fan, "Technical route and typical design reliability analysis of fuze self-neutralization and self-deactivating of cluster sub-munitions," *Acta Armamentatii*, vol. 34, no. 6, pp. 684–689, 2013.

[2] D.-z. Qin, "Relevant concepts of cluster sub-munitions fuze and "three-self " combined design method," *Acta Armamentatii*, vol. 37, no. 2, pp. 239–244, 2016.

[3] C. King, *M85 an Analysis of Reliability*, C King Associates Ltd, Norway, 2007.

[4] S.-S. Feng and Z. H. Wanyan, "Influence of flat-faced submunition's supersonic wake flow on the aerodynamic characteristics of disk-ribbon parachute," *Beijing Institute of Technology*, vol. 31, no. 11, pp. 643–646, 2011.

[5] A. Carruthers and A. Filippone, "Aerodynamic drag of ribbons, parafoils and loops," in *43rd AIAA Aerospace Sciences Meeting and Exhibit-Meeting Papers*, pp. 3297–3307, Nevada, 2005.

[6] W. Yan, F. S.-S. Zhen-Hai, Y. X. Dong, and T. Zhou, "Numerical analysis of flow field characteristics of supersonic submunition with parachute," *Acta Armamentatii*, vol. 32, no. 5, pp. 520–525, 2011.

[7] Z. Tong and F. Shun-Shan, "Effects of distance from projectile base to ribbons-parachute on the system drag performance," *Beijing Institute of Technology*, vol. 33, no. 2, pp. 121–123, 2013.

[8] L. Auman and C. Dahlke, "Drag characteristics of ribbons," in *16th AIAA Aerodynamic Decelerator Systems Technology Conference and Seminar*, Boston, MA, USA, May 2001.

[9] L. Auman, C. Dahlke, and D. Purinton, "Aerodynamic characteristics of ribbon stabilized grenades," in *38th Aerospace Sciences Meeting and Exhibit*, Reno, NV, USA, January 2000.